IVYSPRING INTERNATIONAL PUBLISHER

Theranostics

2018; 8(16): 4393-4408. doi: 10.7150/thno.26869

Review

State-of-the-art of microbubble-assisted blood-brain barrier disruption

Kang-Ho Song[1], Brandon K. Harvey[2] and Mark A. Borden[1]✉

1. Department of Mechanical Engineering, University of Colorado, Boulder, CO 80309
2. Intramural Research Program, National Institute on Drug Abuse, Baltimore, MD 21224

✉ Corresponding author: Mark A Borden, PhD, Department of Mechanical Engineering, University of Colorado, 1111 Engineering Drive, Boulder, CO 80309-0427. Phone: 303.492.7750; Fax: 303.492.3498; Email: mark.borden@colorado.edu

Received: 2018.04.24; Accepted: 2018.07.06; Published: 2018.08.07

Abstract

Focused ultrasound with microbubbles promises unprecedented advantages for blood-brain barrier disruption over existing intracranial drug delivery methods, as well as a significant number of tunable parameters that affect its safety and efficacy. This review provides an engineering perspective on the state-of-the-art of the technology, considering the mechanism of action, effects of microbubble properties, ultrasound parameters and physiological variables, as well as safety and potential therapeutic applications. Emphasis is placed on the use of unified parameters, such as microbubble volume dose (*MVD*) and ultrasound mechanical index, to optimize the procedure and establish safety limits. It is concluded that, while efficacy has been demonstrated in several animal models with a wide range of payloads, acceptable measures of safety should be adopted to accelerate collaboration and improve understanding and clinical relevance.

Key words: focused ultrasound, ultrasound contrast agent, drug delivery, gene therapy

Introduction

In 2005, the World Health Organization reported that the global burden of neurological diseases exceeded that of cancer, HIV and heart disease [1]. The five primary categories of neuropathologies, ordered by frequency, are cerebrovascular diseases (stroke), neurodegenerative disorders (i.e., Parkinson's, Alzheimer's disease), neuroinfections (meningitis, viral infections), brain cancers (glioblastoma, astrocytoma and glioma) [2]; and injuries of the central nervous system (CNS), such as traumatic brain injury [3]. Current examples of invasive drug delivery to the CNS include convection-enhanced delivery (CED, intracranial injection), intracerebral implants (Gliadel® BCNU chemotherapeutic wafers), as well as intraventricular, intrathecal and interstitial delivery (e.g., see needle track in **Figure 1A**). In addition to contributing to extensive recovery periods and cost, invasive procedures pose safety and post-operation quality of life concerns for patients [4].

The brain is one of the most highly vascularized organs in the body, with a capillary density in excess of four times the average found in the human body [5]. Virtually every novel and existing viral and non-viral therapeutic agent targeting the CNS benefits from the ability to pass through the blood-brain barrier (BBB), the primary obstacle to efficient intracerebral delivery of systemically injected therapeutic agents. The BBB primarily comprises brain endothelial cells, basement membrane, pericytes and astrocytes, which interact to form tight-junctions that block the transport of hydrophilic, non-lipophilic, highly charged or large (>400 Da) molecules [6]. The presence of xenobiotic transporters in BBB-specific endothelium further impedes intracerebral drug localization, and accelerates the clearance of drugs already in the CNS to the bloodstream or cerebrospinal fluid [7,8]. The BBB therefore presents a mechanical and chemical obstacle to pathogens and therapeutic agents alike, inducing suboptimal

dose-response and precluding precise drug localization or biomarker targeting of brain parenchymal tissue. Improved trans-BBB drug delivery methods are not only highly desirable, but also necessary to enable cost-effective application of many neuro-therapeutic agents.

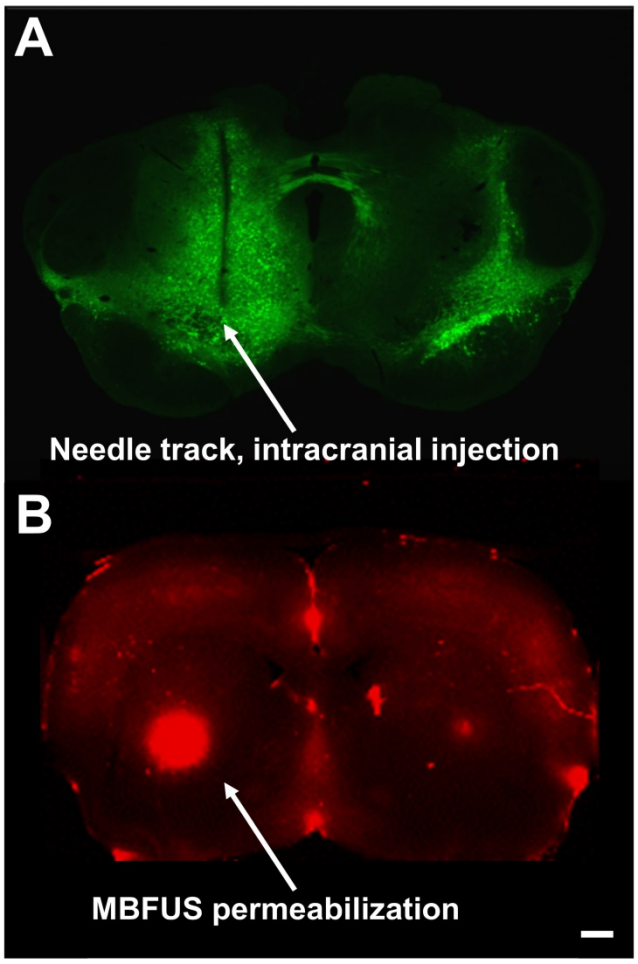

Figure 1. Fluorescence microscopy image comparisons of **(A)** a coronal slice of AAV-EGFP-injected mouse brain with significant needle-track scarring and diffuse area of effect versus **(B)** MB+FUS BBBD in rat brain, demonstrating minimally invasive targeted delivery of systemically injected Evans blue (scale bar is 100 μm).

Blood-brain-barrier disruption (BBBD) aims to compromise transiently the BBB using chemical or mechanical means to allow the passage of circulating therapeutic molecules and biomarkers into, and less frequently, out of the parenchyma (**Table 1**). Chemical approaches to BBBD, such as detergents and receptor-based delivery methods, overcome some of the gross trauma presented by invasive methods, but are faced with the issues of toxicity, minimal control over BBB permeabilization and the certainty of off-target effects. Intra-arterial mannitol infusions, for example, increase cerebral blood flow and improve BBB permeability, but have resulted in 10% mortality due to cerebral edema in studies involving brain cancer therapy and the emergent therapeutic agent, boronophenylalanine [9]. Viral, colloidal, immune and ligand-receptor based delivery schemes aim to circumvent damage done to vascular tissue, but such vehicles are similarly limited in their specificity, affinity and overall ability to deliver sufficient quantities of therapeutic agent [10].

Table 1. Methods of drug delivery to the central nervous system.

		Example	Limitations
Invasive	Interstitial	Direct injection of chemotherapeutic agents into brain tumors, convection-enhanced delivery	Safety—repeated procedures are not well accepted. Scarring evident from needle/catheter
	Intraventricular	Ommaya reservoir	
	Implantables	Gliadel BCNU wafers	Limited drug distribution
Non-invasive	Biological	Peptide masking, prodrugs, viruses	Non-specific, drug alteration
	Chemical	Mannitol	Toxicity, limited efficiency
	Colloidal	Liposomes	Non-specific, low pass-through
	Intranasal	Mucosal grafts	Limited drug distribution

Microbubble-assisted BBBD

Microbubble-assisted focused-ultrasound (MB+FUS) is a particularly attractive noninvasive approach for permeabilizing the BBB due to its tunable and transient effect on vasculature [11], as well as its ability to target specific brain regions using stereotaxic coordinates and image guidance (**Figure 1B**) [12–14]. MB+FUS BBBD offers both chemical and spatial targeting to millimeter-scale resolution, as well as precise temporal control over BBB opening. The microbubbles used in tissue permeabilization are considered theranostic agents, owing to their dual roles as drug-delivery vehicles and highly echogenic ultrasound imaging probes. For example, microbubbles can be used as echogenic "blinking" probes for super-resolution ultrasound imaging of cerebral vasculature [15]. Additionally, the microbubble echo can serve as a signal (e.g., passive cavitation detection) for real-time feedback control [16–18]. Similar to viral, liposomal, nanoparticle- or polymer-based vehicles, microbubbles offer the potential for ligand-receptor targeting [19], payload conjugation and biocompatibility [20,21]. Unlike these conventional delivery vehicles, however, microbubbles offer *in situ* targeting with the use of focused ultrasound (**Figure 2**). Additionally, microbubble-assisted BBBD offers a less invasive alternative to *in vivo* electroporation, and clinical translatability due to its popular use in echocardiography and radiology as an FDA-approved ultrasound contrast agent. Unlike chemical methods of inducing BBBD, varying physical FUS parameters can be used to control the duration of BBB opening [22]. The primary advantage of MB+FUS over its longer-studied predecessor, high-intensity focused

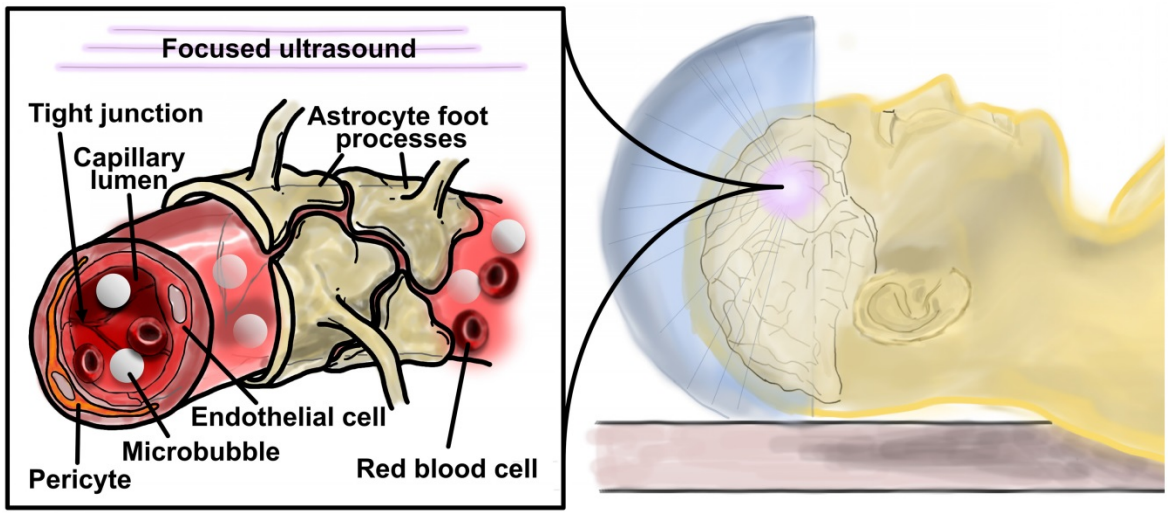

Figure 2. Schematic cartoon of microbubble-assisted focused ultrasound (MB+FUS) blood-brain barrier disruption (BBBD), which uses micrometer-scale mechanofluidic effects from the oscillating microbubbles to enhance drug transport noninvasively, locally and transiently into the brain parenchyma.

ultrasound (HIFU), is the reduced acoustic intensities and temperatures necessary to affect tissue. While HIFU disrupts tissue primarily through heating [23], MB+FUS does so through localized thermomechanical effects [24].

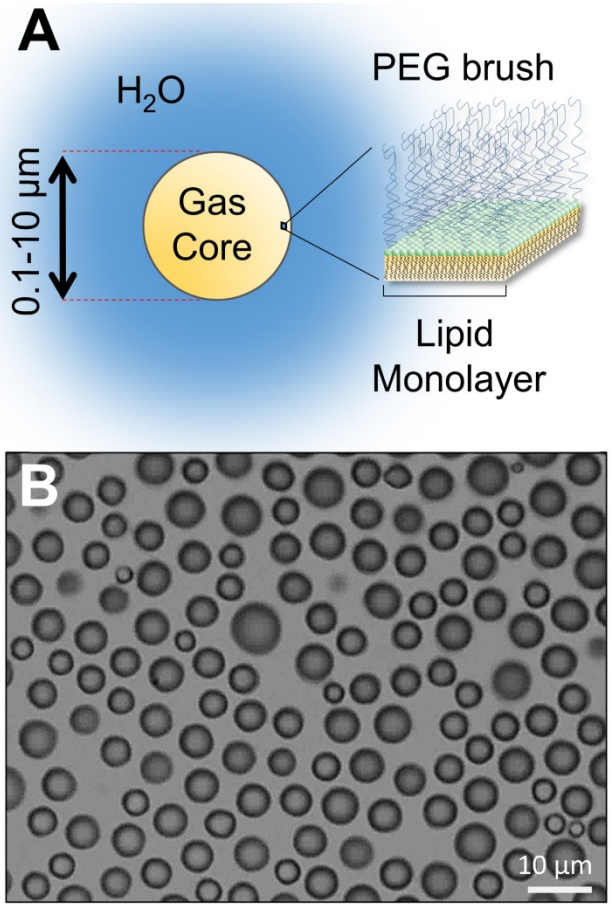

Figure 3. (A) Structure of a lipid-encapsulated microbubble. **(B)** Microscopy image of size-isolated 6-µm lipid-coated microbubbles in suspension.

Mechanism of action

Central to MB+FUS is the acoustic responsiveness of microbubbles, which are 1-10 µm diameter lipid or protein-encapsulated gas spheres (**Figure 3**). Microbubbles excel at transforming kinetic energy from the traveling acoustic wave to the local microenvironment, owing to their high compressibility and tendency to cavitate under ultrasound. When cavitating, microbubbles oscillate volumetrically and induce fluid streaming within a diameter's range away from their surface [25]. Consequently, this oscillation leads to mechanofluidic impingement of nearby cells and tissue, and transient permeabilization.

Acoustic cavitation is typically categorized under two states: stable and transient. Transient cavitation is typified by bubble instability, often accompanied by strong inertial effects such as jetting, fragmentation and shock-wave formation. The latter phenomenon leads to a broadband acoustic emission, often labeled as "inertial cavitation". Inertial cavitation has been suggested as an indicator of cellular damage due to the higher pressures necessary to induce such an event, as well as its destructive effects observed on inorganic materials [26–28]. These inertial events are expected to induce vessel invagination and rupture during MB+FUS BBBD [29–31]. The term "inertial cavitation" is somewhat misleading, however, because so-called "stable" cavitation (typified by prolonged bubble activity) can also lead to high-Reynolds-number inertial effects. Stable cavitation is designated acoustically by harmonic emissions. Stable cavitation can have an equal, if not significantly greater impact on cells, owing to cavitation power persisting over a significantly longer period of time – in essence,

conveying greater overall kinetic energy output compared to shorter duration inertial cavitation [32]. The implementation of passive cavitation detectors (PCDs) has demonstrated the occurrence of BBBD during stable cavitation [33]. Moving from stable to inertial cavitation was shown to induce larger molecular weight delivery [34]. Additionally, MB+FUS-mediated changes in the gene expression of key BBB efflux transport proteins, such as downregulation of P-glycoprotein, may significantly alter the pharmacokinetics of BBBD, improving drug localization in the parenchyma [35,36]. Owing to the inability to directly observe microbubble activity at the BBB *in vivo* at tissue depth, however, no study so far has isolated the exact physical mechanism of stable cavitation on BBBD.

Due to the microscale influence of cavitation from microbubbles [25], concerns have been expressed regarding the fate of therapeutic agents after extravasation from intracranial vasculature, specifically the hypothesized inability of MB+FUS to disrupt the brain parenchyma in addition to vasculature [22]. With an average capillary density of 600 per mm^3 throughout the body, human cells conservatively reside within two or three cell-lengths (120-180 μm) from the nearest capillary [5]. The brain has an average capillary density of 2500-3000 capillaries/mm^3, suggesting that a significant portion of brain cells are within 100 μm of the nearest capillary [37]. To address concerns regarding inefficient drug diffusion into the parenchyma, we can estimate drug penetration through 100 μm of cerebral tissue using diffusion parameters for a potential payload: glial cell-line derived neurotropic factor (GDNF). GDNF is an 18-kDa protein that does not efficiently cross the BBB but has potent trophic actions for treatment of Parkinson's disease and other neurodegenerative disorders. We can predict the adequate tissue distribution of GDNF originating from a capillary and traversing through the brain parenchyma using a previously proposed diffusion model of therapeutic agents in brain tissue [38]:

$$\frac{C}{C_0} = e^{-x\sqrt{ln2/(\tau D^*)}}$$

where C_0 is the concentration at either the periventricular or pial brain surface (x = 0), C is the concentration in tissue at a distance x from source, τ is the efflux half-life (72 h for GDNF) and D^* is its diffusion constant corrected for brain tortuosity (1.3×10^{-6} cm^2/s for GDNF) [38–40]. Using this model, the concentration fraction (C/C_0) of GDNF 100 μm from the capillary is estimated to be 98.6%. This calculation for the macromolecule GDNF supports the argument that BBBD is sufficient for effective drug delivery to the brain.

MB+FUS BBBD is affected by several independent variables, which can be classified as microbubble, acoustic and physiological parameters (**Figure 4**). Of these, acoustic parameters have been extensively studied both *in vitro* and *in vivo*, while studies on the effect of microbubble and physiological parameters remain sparse. These parameters can have significant effects on the magnitude and duration of BBBD, tissue damage, immune response and drug distribution.

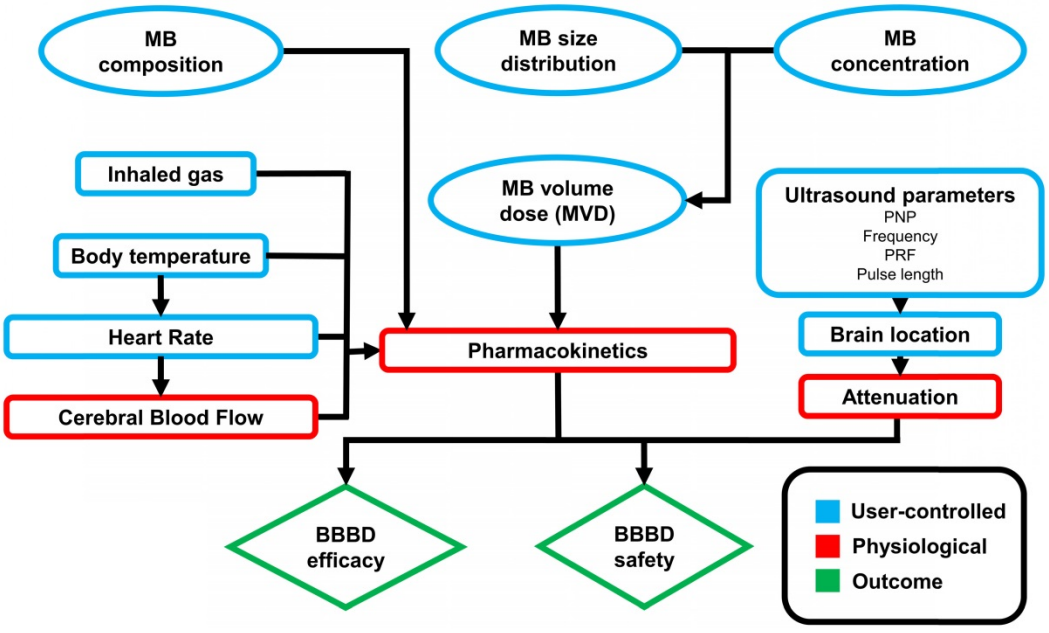

Figure 4. Parameters affecting MB+FUS BBBD outcome.

Microbubble parameters

Ultrasound contrast agents (UCAs)

Many studies rely on FDA-approved ultrasound contrast agents (UCAs), which were originally developed for echocardiography, because they are commercially available and have already received regulatory approval for diagnostic imaging. Examples of commonly used UCA formulations include Optison™ (GE Health Care), Definity® (Lantheus Biomedical) and SonoVue® (Bracco Imaging): one protein and two lipid-shelled microbubbles, respectively. In addition to differences in microbubble shell mechanics and transport properties, these UCAs also exhibit significant differences in microbubble gas composition, concentration and size distribution from each other. Differences in microbubble concentration and size exist even among batches of the same formulation (hence, a range of sizes is given on the product inserts) [41]. While these differences are inconsequential for qualitative contrast-enhanced ultrasound imaging, they are all known to significantly affect MB+FUS tissue permeabilization [14,32,41,42]. Thus, while it is tempting to use UCAs for BBBD studies owing to the obvious benefit of having already received regulatory approval, the agent-to-agent and batch-to-batch variability may ultimately hinder regulatory approval of MB+FUS BBBD and broad dissemination of the technology. We need to improve our understanding of these microbubble properties and, in turn, how they affect the safety and efficacy of BBBD.

Indeed, agreement on optimized reference parameters has remained difficult to achieve in MB+FUS BBBD studies [43,44]. This is due in part to difficulty in standardizing the microbubble dose (**Figure 5A**). In most studies, dose is reported as volume of stock formulation injected per weight (mL/kg) of the subject. We define this dose as the fluid volume dose (*FVD*), which is defined as:

$$FVD = V_{stock} / m_{subject}$$

where V_{stock} is the volume of fluid taken from the stock solution and injected into the subject, and $m_{subject}$ is the mass of the subject. Despite the prevalent use of FVD in the literature, this form of the dose is disadvantaged by the variation in gas composition, shell properties, microbubble concentration and particle size distribution. These variations make it extremely difficult to correlate the effects of FVD to the resulting measures of MB+FUS effects. Indeed, MB+FUS BBBD dosing parameters remain central to understanding the different presentations of sterile immune response (SIR) in the brain—a matter of some

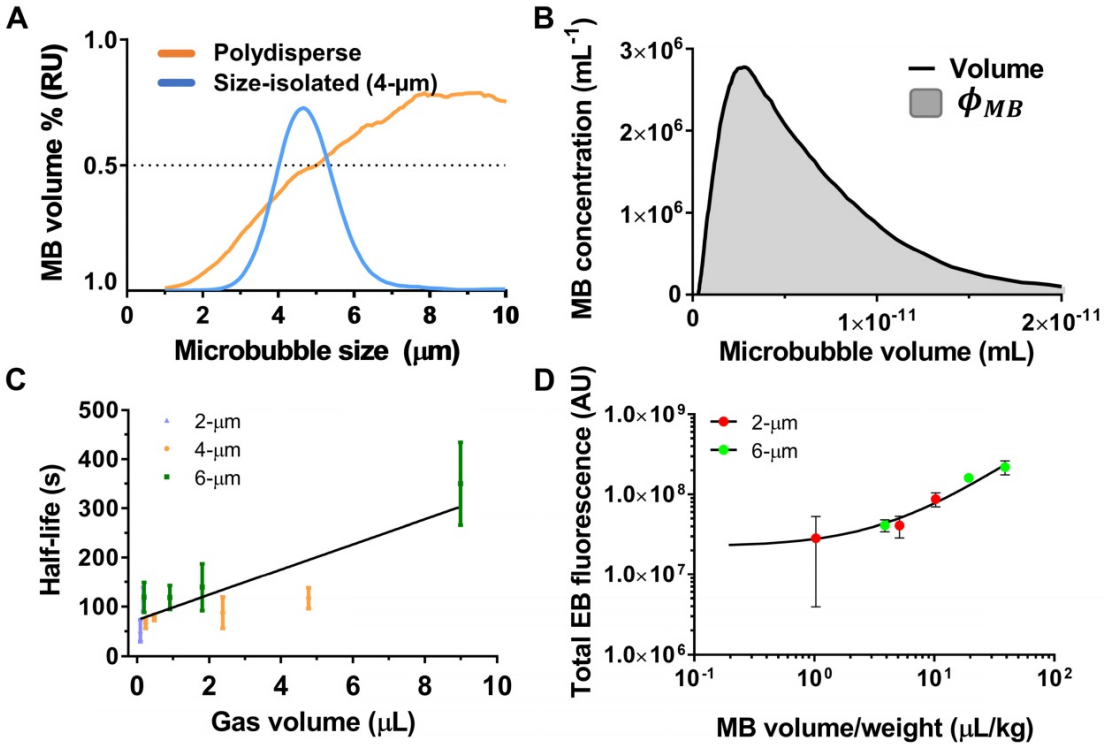

Figure 5. (A) Microbubble volume-weighted size distributions for polydisperse vs. size-isolated 4-μm lipid-coated microbubbles. **(B)** Microbubble concentration versus volume. The area under the curve is equal to φ_{MB} (equation 4 in the text) and used to calculate the microbubble gas volume dose (*MVD*). **(C)** Microbubble *in vivo* circulation half-life as a function of *MVD* after systemic delivery of 2-, 4- and 6-μm size-isolated, lipid-coated microbubbles in CD-1 mice under ultrasound imaging (Vevo 770; Visualsonics) [52]. **(D)** Extravasated Evans blue fluorescence in the striatum after MB+FUS BBBD as a function of *MVD* for 2- and 6- μm size-isolated, lipid-coated microbubbles in adult Sprague-Dawley rats [14].

debate [45,46], which centers on whether or not there is a therapeutic window between the microbubble concentration needed to induce BBBD and that which causes SIR. Even matching FVD and acoustic parameters, two studies using different UCA formulations will likely observe significant differences in results due to unequal microbubble concentration, size distribution, gas composition and shell chemistry [47].

Microbubble dose

Among the first MB+FUS BBBD parameters studied after acoustic intensity was microbubble dose [48]. Early studies often used commercial UCA formulations and treated microbubble dose similar to drug dose: representing varying microbubble dose as *FVD* [49]. Precedent, as well as the availability of pre-formulated UCAs, may explain the continued use of *FVD* in MB+FUS BBBD studies today [45,50]. As mentioned previously, however, commercial UCAs can differ significantly in composition, size and concentration, even between vials of the same brand [41]. There exists strong evidence that this may introduce variability in BBBD [51–53]. Beyond the possibility of identifying *optimized* microbubble size distributions and concentrations, unified parameters such as total microbubble gas volume allow for retroactive and future overlap between studies [14]. We therefore recommend the use of "microbubble volume dose" (*MVD*), which is defined as follows:

$$MVD = FVD \times \phi_{MB}$$

where φ_{MB} is the volume fraction of the stock solution that is occupied by microbubbles (**Figure 5B**). The value of φ_{MB} is a function of the particle size distribution (PSD); it can be determined by plotting the microbubble number concentration (c) versus microbubble volume (v) and integrating to find the area under the curve.

$$\phi_{MB} = \int_0^\infty cdv$$

The utility of *MVD* is that it captures both microbubble size and concentration in a single variable. We recently showed the utility of *MVD* in a study examining BBBD efficiency in adult rats sonicated at 1.0 MHz center frequency and 0.5 MPa peak negative pressure (PNP) de-rated for skull attenuation [14]. Size-isolated microbubbles with diameters of 2 or 6 µm were injected at number doses ranging from 4×10^7 to 4×10^8 MB/kg. As found in a previous investigation, increasing injected microbubble size and count increased permeability [51]. However, conversion of both parameters to *MVD* yielded a clear, linear indicator of BBBD magnitude, regardless of microbubble size or count. The trend between integrated fluorescence intensity of Evan's blue dye in the brain parenchyma and *MVD* was linear, with different microbubble sizes collapsing to the same linear trend line.

The advantage of *MVD* over *FVD* is that it provides a unified dose metric for each injection [41]. Similarly, deducing the *MVD* retroactively may allow for the useful comparison of previously investigated BBBD variables, such as acoustic and physiological parameters, as long as UCA concentrations and size distributions are known. Values of φ_{MB} and *MVD* for common UCAs at the recommended dose for diagnostic imaging are tabulated here to facilitate such comparisons (**Table 2**). One can implement *MVD* into the guidance and control of drug delivery by taking the following steps:

Table 2. *MVD* of common UCAs at the dose recommended for diagnostic imaging.

Product	φ_{MB} (µL/mL) [a]	*FVD* (µL/kg) [b]	*MVD* (µL/kg)
Optison	35.2 ± 3.0	6.2	0.22
Definity	44 ± 9.5	10	0.44
Sonovue	6.5 ± 1.2	25	0.16

[a] Taken from Hyvelin et al. [113]. [b] Taken from product inserts for an average adult human. φ_{MB} is microbubble volume fraction, *FVD* is fluid volume dose, *MVD* is microbubble volume dose.

1. Measure the particle size distribution and concentration using an accurate method, such as the Coulter principle [54,55]. Ideally, this is done just prior to injection, as dilution and handling can alter the total number and size of the microbubbles.

2. Convert the size distribution to microbubble number concentration versus microbubble volume ($V = \frac{4}{3}\pi R^3$) and integrate to determine φ_{MB}.

3. Multiply φ_{MB} by the indicated *FVD* to determine *MVD*.

Of course, changing other parameters (e.g., microbubble surface charge, drug size, ultrasound parameters etc.) may shift the curves of *MVD* vs. drug delivery. More research is necessary to better understand these effects.

More investigation into the linearity of BBBD vs. *MVD* is also warranted. Several factors may hypothetically alter this trend. For example, the slope of the trend line may shift over a range of *MVDs* corresponding to a change in the dominant pathway for microbubble elimination (phagocytosis vs. dissolution). Additionally, BBBD may saturate and even decrease as *MVD* is increased to a point where MBs significantly attenuate the FUS beam in tissue between the transducer and focus. Future work is necessary to elucidate these effects.

Microbubble pharmacokinetics

Upon injection, microbubbles circulate systemically until stimulated at the target site by

ultrasound. Microbubble circulation persistence is known to depend on microbubble dissolution rate and the rate of clearance by the mononuclear phagocyte system. Microbubble dissolution rate is affected by properties of the individual microbubble, such as size and gas/shell composition, as well as the ensemble (concentration and size distribution). For example, well-established models of single microbubble dissolution [56], as well as data on suspensions from *in vivo* imaging studies [52], suggest that increasing microbubble diameter and/or concentration significantly increases circulation persistence (**Figure 5C**). As for BBBD, a linear relationship was observed between microbubble half-life ($\tau_{1/2}$) and *MVD*. In addition to providing longer imaging windows, enhanced circulation persistence may increase microbubble concentration at the targeted site during the treatment, increasing permeabilization. Previous results obtained by O'Reilly et al. indicate that BBBD correlated with peak circulating microbubble concentration [57]: short-duration (15 s) bolus injections consistently effected greater BBBD than long-duration (2 min) injections of the same microbubble dose, likely due to a lower peak concentration of MB in the circulation for the latter. Clearly, more work is necessary to establish the role of both MB and drug pharmacokinetics on MB+FUS BBBD, and this could be facilitated by use of *MVD* in dosing.

Microbubble size

Microbubble size has been linked to increased tissue permeabilization [51]. A notable study on the effect of microbubble size on a popular measure of BBBD, quantification of extravasated magnetic resonance imaging (MRI) contrast agent, was conducted by Samiotaki et al. in mouse models, using 2-, 4- and 6-μm diameter microbubbles [53]. Although the primary aim of the study was to identify the rate at which the BBB healed after BBBD, several peripheral results provided compelling support for the implementation of monodisperse microbubbles to improve control over treatment. A 1.5-MHz focused ultrasound array was targeted to the area between the hippocampus and the thalamus on the right hemisphere for 60 s, using 10 Hz pulse repetition frequency (PRF), 60 μs pulse length and 0.3-0.6 MPa PNP. The results showed that BBB healing occurred in the reverse of permeabilization, starting at the outer edges of the treatment region and moving towards the center. Significantly less BBBD was seen with the smaller 2-μm microbubbles as opposed to 4- and 6-μm microbubbles. Additionally, the time for BBB closing was dependent on microbubble size. Previous studies had shown that the time of BBB closing was approximately 24-48 h with polydisperse commercial formulations [53]. FUS with larger microbubbles (4- and 6-μm) increased the duration of BBBD to over five days. The authors explained this result as being a consequence of larger pores created by larger microbubbles. Additionally, tissue damage (dark neurons, extravasated red blood cells) seen initially with short time-course studies was not observed, or greatly mitigated in the mice, suggesting that disrupted tissue may recover after a few days. However, this study compared size effects at a common microbubble *number* dose (*MND* in units of *MB/kg*) rather than *MVD*, making it difficult to distinguish the relative impact of number versus size. It therefore remains unclear whether or not microbubble size affects the extent of BBBD when isolated from effects of *MVD*. Preliminary data by Song et al. for cationic lipid-coated microbubbles indicate that it does not [14], but more work is necessary to confirm this result.

Microbubble composition

Typical UCA formulations use albumin protein (Optison) or phospholipids (Definity and Sonovue). While clinical microbubbles are expedient for rapidly moving the technology to clinical trials, many researchers believe that UCA compositions originally developed for diagnostic imaging are suboptimal for BBBD. However, very few studies have systematically investigated the effect of microbubble composition on the measures of BBBD. Wu et al. examined the effects of lipid acyl chain lengths C16, C18 and C24 for size-isolated microbubbles on BBBD using 1.5 MHz frequency and 0.23 to 0.6 MPa PNP [47]. Interestingly, increasing microbubble tail length resulted in a significant increase in 70-kDa fluorescent dextran extravasation, while insignificant differences were seen for 3-kDa dextran. This suggests that microbubbles comprising longer acyl-chain lipids, which are known to circulate longer *in vivo* [58], may favorably affect delivery efficiency of larger drug molecules. The composition of the gas core has been shown to dictate circulation persistence due to varying solubility and diffusivity [59,60], but few other bioeffects have been linked to gas composition. We suggest that effects of composition on pharmacokinetics and BBBD should be isolated from size and concentration by the use of *MVD*.

Microbubble complexes have been engineered for improved control over BBBD and subsequent drug delivery. In a study conducted by Åslund et al., nanoparticle-coated microbubbles were shown to direct delivery to the brain [61]. The same group showed that a UCA conjugated to a lipid-encapsulated perfluoromethylcyclopentane droplet

induced droplet vaporization under FUS, generating temporary >25 μm microbubble complexes that transiently occluded blood flow for up to 10 min [62]. Burke et al. demonstrated that MB+FUS with agents comprising 5-fluorouracil-bearing nanoparticles bonded to microbubbles inhibit solid glioma tumor growth and improve survival [63]. Clearly, more research is warranted to optimize microbubble design and complexation for BBBD applications.

Summary of microbubble effects

Figure 4 shows a simplified block flow diagram displaying the influence of microbubble parameters on MB+FUS BBBD. As we describe above, microbubble concentration and size distribution can be combined into a single dose parameter: the microbubble volume dose (*MVD*). Both microbubble composition (gas and shell) and dose are expected to affect the pharmacokinetics (circulation half-life and area-under-the-curve). Note that physiological (e.g., immune competency) and ultrasound (e.g., stable *vs.* transient cavitation) parameters also may affect the pharmacokinetics. In turn, the microbubble pharmacokinetics and ultrasound parameters determine the safety and efficacy of MB+FUS BBBD.

Physiological parameters

Skull attenuation

Perhaps the first obstacle facing translation of MB+FUS BBBD to the clinical setting was transmitting sufficient and precise ultrasonic energy through the skull to the brain tissue within. The pressure amplitude is diminished by attenuation from the transducer, coupling agent, skin, skull and brain tissue beneath, as well as reflections at the boundaries between them. The ratio by which the transmission is decreased can be estimated by the following equation [64]:

$$T = \frac{P}{P_0} = \frac{2Z_2}{Z_1 + Z_2} \cdot \frac{2Z_3}{Z_2 + Z_3} \cdot e^{-\alpha_2 f x_2 / 8.7}$$

Where T is the overall pressure amplitude transmission coefficient; P_0 and P are the pressures transmitted by the transducer and into the brain, respectively; Z_1, Z_2 and Z_3 are the acoustic impedances for skin [1.99 x 10^{-6} kg/(s·m^2)], bone [7.75 x 10^{-6} kg/(s·m^2)] and brain tissue [1.60 x 10^{-6} kg/(s·m^2)], respectively; a_2 and x_2 are the attenuation [20dB/(cm·MHz)] and thickness (6 mm in humans and 0.5 mm in rats) of the bone [65]; and f is the frequency of the acoustic pulse (MHz). This calculation gives a transmission coefficient of approximately 14% in humans and 50% in rats, which are in line with experimental results [66,67].

The challenges posed by the skull in larger animals regarding MB+FUS were first reported by McDannold et al. in a 2010 conference proceeding [68], and then by Tung et al. in 2011 [69]. In the latter, three macaque monkeys were treated with 500 μL of Definity (1.1-3.3 μm diameter) or 4-μm diameter size-isolated lipid microbubbles. The 18-cm transducer, driven at 500 kHz and 0.3 or 0.45 MPa, failed to induce BBBD with Definity microbubbles. BBBD was seen, however, with the size-isolated microbubbles, and in subsequent studies with Definity by McDannold et al. [70], who utilized a 30-cm Exablate 4000 (Insightec) 220-kHz hemispherical FUS transducer array, suggesting that lower driving frequencies and increased transducer area may aid in achieving BBBD at mechanical indices (see the section 'Mechanical index') as low as 0.32 (149 kPa PNP).

Brain location and vasculature

In the non-human primate study mentioned above [69], the results showed that BBBD was not visible at some acoustic intensities that induced inertial cavitation (recorded with a passive cavitation detector). These occurrences coincided with the localization of MB+FUS in sinuses within the brain tissue, which suggested that the cavitating microbubbles were unable to impinge efficiently upon the endothelium when stimulated in these relatively large fluid regions, as opposed to smaller diameter vessels. Treatments at 0.3 MPa PNP effected more BBBD than 0.45 MPa sonications owing to variation in location, suggesting that the vascular structure at the treatment region is an important consideration.

The type of vasculature affected by MB+FUS has also been shown to affect BBBD [71]. A 2006 study by Sheikov et al. indicated that arterioles, the intermediate vasculature between arteries and capillaries, demonstrated more trans-endothelial transport compared to capillaries and venules. As opposed to vascular compromise, the primary means of marker transfer into the parenchyma was reported to be transcytosis at 0.69 and 0.26 MHz with an estimated target-site acoustic pressure of 0.3-0.8 MPa and Optison microbubbles. Future studies will likely need to optimize not only FUS parameters, but also MB dose, when choosing a specific target in the brain for drug delivery.

Anesthesia carrier gas

Microbubble dose at the target site is affected by a combination of microbubble dissolution and clearance in specific organs, namely the lungs, liver and spleen [52,72]. Some of these factors can be expediently controlled through microbubble parameters [58]. However, the partial pressures of

dissolved gases in the blood, which are directly affected by inhaled gas composition and physiology of the cardiopulmonary circuit, have also been shown to control microbubble circulation persistence [45,50]. Longer microbubble persistence was observed in animals breathing air as the anesthesia carrier, in comparison to oxygen, owing to nitrogen gas and lower ventilation/perfusion mismatch.

Additionally, it is known that decreasing pO_2 can trigger the formation of adenosine and other potent vasodilators, increasing cerebral blood flow and likely the concentration of microbubbles at the target site [73]. Results by McDannold et al. may corroborate this effect, as BBBD in mice injected with Optison and targeted with 690 kHz 0.54 MPa PNP showed a significantly greater volume of BBBD (as quantified by MRI) after inhaling 21% (air) vs. 100% O_2 [74]. The partial pressure of oxygen in the blood can affect heart rate as well [73], a physiological parameter that can differ greatly between species and individuals, and the effects of which are unexplored regarding MB+FUS BBBD. In rats, for example, the resting heart rate is 330-480 bpm [75], while the resting heart rate in humans falls within 60-100 bpm, which may significantly alter the availability and clearance of microbubbles before and during BBBD.

Ultrasound parameters

Before the incorporation of microbubbles, ultrasound parameters were among the first to be examined in the context of BBBD. The use of ultrasound alone to effect BBBD was first demonstrated by Lynn et al. in 1942, and by Bakay et al. in 1956 [76,77]. Although this new method was non-invasive and could spatially target treatment regions deep within the body, the resulting cell death and tissue damage limited translatability. It was almost 55 years before the first exogenous microbubble-assisted permeabilization of the BBB was conducted by Hynynen et al. in 1996, with acoustic parameters as the focus of investigation [78]. These early microbubble studies demonstrated that BBBD could be achieved with much lower acoustic amplitudes than with ultrasound alone, greatly reducing the risk of neuronal and parenchymal tissue damage [24,78,79], and enabling a greater variety of effects beyond local heating. Although these early studies examined the effect of varying ultrasound parameters, it is important to consider the significant interaction between acoustic, microbubble and physiological parameters as outlined below.

Mechanical index (MI)

Mechanical index (*MI*) is a parameter unifying ultrasound frequency (*f* in units of MHz) and acoustic pressure (*PNP* in units of MPa) through the following relationship:

$$MI = \frac{PNP}{\sqrt{f}}$$

While several studies indirectly examined mechanical index by varying acoustic pressure or frequency alone, few studies have examined the effect of mechanical index by varying *both* pressure and frequency. Experimental results from Chu et al., as well as collated results from other groups, indicate that *MI* correlates well with BBBD efficiency over a range of PNPs and frequencies (0.41-1.12 *MI*; 0.25-0.83 MPa; 0.4-1.0 MHz) [80]. However, few studies have measured *MI* at the target site due to the heterogeneity of intervening and targeted tissue in MB+FUS BBBD. Early *in vitro* studies of microbubbles demonstrated that inertial cavitation occurs at *MI* as low as 0.5, although it is important to note that several studies in adult rats (250+ g) demonstrated effective BBBD at *MI* as low as 0.25 (0.125 estimated in adult rats, see the section 'Skull attenuation'), showing that stable cavitation is sufficient to induce BBBD [16,70,81,82]. An *MI* of 0.45 was identified by several studies as a safe and effective threshold for BBBD [16,70,81,82,80], although this does not account for the effect of microbubble parameters, sonication duration or immune response. For example, increasing the number of ultrasound cycles at a fixed *MI* has been shown to significantly increase BBBD [69], and significant immune response has been observed at *MI* under 0.4 [45,50].

Pulse center frequency

In addition to affecting mechanical index, the pulse center frequency affects cranial attenuation. While *in vitro* studies with macaque (attenuation: 4.92 dB/mm) and human skull samples (7.33 dB/mm) have demonstrated that lower frequency ultrasound corresponds to decreased attenuation [83], no study to date has isolated this effect on BBBD efficiency. It is important to note that studies using low-frequency ultrasound (~300 kHz, 700 mW/cm^2; ~0.19 MI) alone have resulted in undesired cerebral hemorrhaging in patients and animal models (~20 kHz; 0.5 W/cm^2; ~0.61 MI) [84,85].

The MB+FUS effects, independent of *MI*, are in principle closely related at the microbubble resonance frequency. Microbubble resonance frequency has been reviewed by Doinikov et al. [86]. The linearized resonance frequency (f_0) for small-amplitude oscillations of lipid-shelled microbubbles is given by [87]:

$$f_0 = \frac{1}{2\pi R_0}\sqrt{\frac{3\gamma p_A}{\rho} + \frac{2(3\gamma - 1)\sigma_w}{R_0} + \frac{4\chi}{R_0}}$$

where R_0 is microbubble resting radius, γ is the polytropic coefficient, p_A is ambient pressure, ρ is the density of the medium, σ_w is surface tension and x is lipid shell elasticity. The nonlinear acoustic behaviors of forced bubble oscillation are dependent on the mismatch between the microbubble resonance frequency and the driving frequency, the acoustic pressure and microbubble distribution in the insonified area. Therefore, isolating the effects of frequency necessitates the use of monodisperse microbubbles at matched mechanical index and *MVD*. Such a study has yet to be reported in the literature.

Peak negative pressure (PNP)

Due to attenuation and limited transducer bandwidth, varying PNP offers a more expedient means of altering *MI* and the magnitude of BBBD. Early MB+FUS BBBD studies exclusively focused on the effects of acoustic driving pressure and acoustic intensity [24,78]. The acoustic attenuation differs between animal models, but clear trends exist between increasing acoustic pressure and its bioeffects, although the effects of varying PNP alone, independent of *MI*, are unclear. It is generally well-established that increasing acoustic pressure increases the relative expansion and wall velocities of microbubbles, and is thus linked to increased BBBD as well as BBBD-related effects such as petechiae formation [24,78,88,17].

An acoustic output-control scheme currently used in at least one clinical trial is the feedback-facilitated adjustment of PNP to induce stable-cavitation-mediated BBBD [16,18]. This approach was demonstrated by O'Reilly et al. in 2012, and by Sun et al. in 2017, under the assumption that inertial cavitation would cause tissue damage, and that stable cavitation was favorable [16,17] . In contrast with previous studies on MB+FUS BBBD, which linked absolute PNP values to BBBD efficiency and safety, a percentage pressure threshold of 50% of the minimum PNP necessary to induce inertial cavitation was identified as efficacious and safe at a frequency of 551.5 kHz. This method revealed that peak pressures as low as 0.18 MPa (likely corresponding to stable cavitation) induced BBBD, while the highest peak pressure that disrupted the BBB without causing tissue damage, as indicated by NeuN stains and macroscopic analysis, was 0.40 MPa—a value corroborated by previous studies in adult rats [16,70,81,82,80]. Increasing the pressure threshold from 50% to 75% was enough to induce frequent edema, underscoring the variable and narrow range of PNPs able to induce non-superfluous BBBD in individual animals. In the context of safety, it is important to note that MRI of animals in which edema was detected immediately after sonication showed no signs of edema eight days after MB+FUS BBBD. This type of feedback control is currently in use in clinical trials.

Pulse repetition frequency (PRF) and pulse length

In comparison with mechanical index and frequency, the effects of pulse repetition frequency (PRF) and pulse length have received less attention. In general, a simultaneous increase in PRF and pulse length (*N* number of cycles per pulse; *T* time per pulse) is expected to increase BBBD by increasing duty cycle [89]:

$$\%DC = PRF \cdot T \cdot 100\%$$

However, physiological responses to the stress of MB+FUS have been shown to also be affected by "resting periods", as demonstrated by Choi et al. [89]. Contrary to early results obtained by McDannold et al. [82], these studies demonstrated that PRF plays a significant role in BBBD efficacy: resting periods shorter than 0.1 s or longer than 1 s (1.5 MHz) resulted in no BBBD. While increasing pulse length has been shown to improve model drug penetration into the parenchyma [82], it has also been hypothesized that long pulse lengths increase the occurrence of standing waves, inducing off-target effects and increasing tissue damage [13,89].

Safety considerations

BBBD safety has been a long-standing concern related to the standardization of ultrasonic and microbubble parameters. Qualitative assessments of excised neural tissue (evidence of dead or compromised parenchyma) and quantitative assessments of behavior (motor function after recovery period) have been the most common means of evaluating BBBD safety [70,89,90]. The field of MB+FUS BBBD has only recently begun to introduce multi-reporter immune-histo-fluorescence (IHF) to monitor immune response, vascular structure and cell death. In contrast, the safety of potential pharmaceutical agents is often comprehensively evaluated with quantitative immunostaining, high-throughput imaging and relevant functional tests; for motor function, studies often included rotarod performance, grip-strength tests and behavioral assays such as the Basso-Beattie-Bresnahan locomotor rating scale for rats, and Basso Mouse Scale for mice.

Some studies have observed the presence of petechiae, or visually detectable extravasated red blood cells [90,88,13,74]. Contradictory interpretations

regarding the impact of petechiae on safety have been presented. Another early mode of examination of BBBD safety was qualitative observations of hemorrhage and edema as indicated by MRI imagery [24]. In MRI-guided focused ultrasound (MRIg-FUS), edema and hemorrhage are indicated by increased blood flow by MRI image processing to the regions of exposure. While several MRIg-FUS studies have suggested that such results demonstrate effective BBBD with minimal or no hemorrhaging, low level of hemorrhaging has not been conclusively evaluated. Although blood toxicity is a well-studied phenomenon in cases of stroke, cerebrovascular insults (compared to MB+FUS) represent significantly larger quantities of blood and red blood cells accumulating in the parenchyma, with accompanying pressure, clotting and other bulk effects. Indeed, the effect of just heme and other erythrocyte components is poorly understood [91]. The effect of micropetechiae seen in MB+FUS BBBD on neuronal health is unstudied. However, it makes sense that in the case of BBBD, micropetechiae are a byproduct of transiently compromising cerebral vasculature to induce macromolecular delivery. MB+FUS BBBD behavioral studies have also reported that despite the presence of edema or petechiae immediately after BBBD in macaques, they were not present one week later [90]. It is important to emphasize that the presence of petechiae may not be evidence of trauma post-BBBD. Although petechiae are often present in cases of brain jury, sufficient BBBD for passage of drugs and biomolecules may be accompanied by extravasation of red blood cells.

A complementary means of evaluating neuronal insult is immunostaining for activated immune cells, specifically, microglia. Microglia are the primary immune cells in the brain and are critical for monitoring the brain for pathogens and foreign molecules, as well as responding to injury. Activation of microglia is readily detected using antibodies to cell markers, such as anti-Iba1 (**Figure 6**). Unlike qualitative assessments of neuronal health, studies of immune cells have demonstrated significant immune cell response to BBBD [50]. Additionally, pro-inflammatory cytokines such as interleukin-1, tumor necrosis factor alpha (TNFα) and heat shock protein (hsp) 70 can be interrogated with immunostaining, as well as by RNA expression profiling of treated brain tissue. In RNA expression profiling, mRNA from treated tissue is quantified and compared to untreated tissue to indicate changes in the cellular transcriptome due to BBBD. A handful of studies have examined cellular stress in this manner [45,50]. In 2017, Kovacs et al. published an article examining sterile immune response (SIR) as an aggregate of Iba1 expression using anti-Iba1 reporter molecules, presence of pro-inflammatory and anti-inflammatory cytokines, chemokines and trophic factors (CCTFs), macrophage presence and differential gene mapping examining components of NFκB-mediated inflammation. Significant increase in Iba1 expression as indicated by anti-Iba1, as well as mRNA related to NFκB-associated genes were increased following MB+FUS BBBD at 590 kHz, 0.3 MPa with Optison in rats. Cellular insult immediately after BBBD was apparent in elevated levels of HSP70 and pro-inflammatory cytokines (interleukins etc.) at the target site, an inflammatory response that subsided after 24 h. Activated astrocytes and microglia were still present six days after the study. On the other hand, McMahon et al. [45] showed that SIR is dependent on MB dose, sparking an important

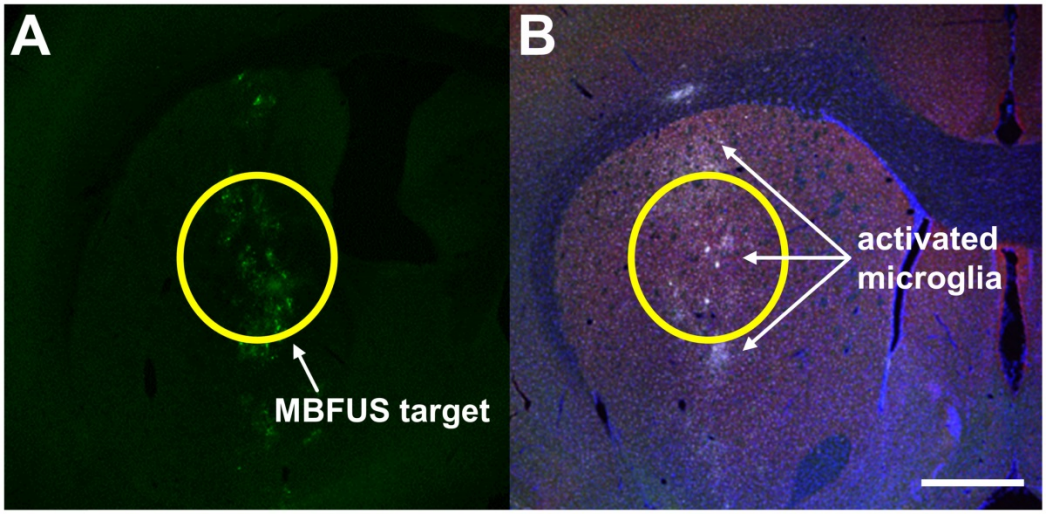

Figure 6. (A) dsAAV1-CMV-eGFP transduction (green) after MB+FUS BBBD using 6-μm SIMBs (2×10^8 MB/kg) in adult 350 g female Sprague-Dawley rats. A Philips Therapeutic Imaging Probe System was utilized to target the right striatum at 1 MHz, 0.5 MPa PN, 100 Hz PRF and 10% duty cycle [14]. **(B)** Iba1 immunostaining of inflamed microglia (white) after MB+FUS BBBD of the targeted region (scale bar is 100 μm).

debate over the role of MBs in BBBD and SIR [46,92], and highlighting the importance of aforementioned considerations detailed in this review.

Behavioral studies are another fundamental component in the study of therapeutic neurologic agents, ranging from fine motor control tests to behavioral scoring. Studies on macaques indicated that two minutes of FUS applied at 0.3 and 0.55 MI with 4-5 μm size-isolated microbubbles resulted in effective BBBD accompanied by degraded reaction time and visual motion discrimination immediately after sonication. However, animal cognitive performance was reported to return to baseline four days after sonication [90]. A similar study was conducted by Olumolade et al. at 1.5 MHz, 0.45-1.5 MPa examining rotarod and open field performance in 8-week-old (adolescent) mice. While functional deficits were observed immediately after BBBD for the positive control group, no significant differences in rotarod or open field tests were observed after four weeks at 0.45 MPa or 1.5 MPa PRP (positive control).

Therapeutic and clinical applications

In addition to potential diagnostic roles, microbubbles and MB+FUS are particularly suited to therapeutic applications (**Table 3**). MB+FUS overcomes significant deficits and augments strengths in existing therapeutic agents and existing schemes of drug localization, such as enhanced permeability and retention (EPR), in which drug particles accumulate in convoluted vasculature, or nanoparticle and polymer-based delivery [93]. Additionally, MB+FUS BBBD may overcome insufficient trans-BBB performance of many promising therapeutic agents and address the lack of a true targeting scheme, as well as reducing the magnitude of off-target effects. Currently, at least two MB+FUS clinical trials are underway: one for the treatment of brain cancers using Definity and a custom FUS array [94], and the other using Sonovue and an implantable ultrasound system, SonoCloud [95].

Table 3. Therapeutic agents delivered with MB+FUS in animal models.

Delivered agent	Proposed application	References
Adeno-associated virus	Gene therapy	[108–112,14]
Anti-Aβ	Alzheimer's disease	[96,98,99]
BCNU	Chemotherapeutic	[114,115]
Boronphenylalanine	Chemotherapeutic	[116,104]
Doxorubicin	Chemotherapeutic	[100,117]
Epirubicin	Chemotherapeutic	[93]
GDNF	Parkinson's disease, TBI	[118,119]
Herceptin	Chemotherapeutic, metastatic breast cancer	[120]
Htt-siRNA	Huntington's disease	[121,122]
Methotrexate	Chemotherapeutic	[123]
Stem cells	Neuroregeneration	[124]
Temozolomide	Chemotherapeutic	[125]

Targeted therapy and molecular diagnostics in particular, have much to gain from the utilization of MB+FUS BBBD. Today, at least 118 monoclonal antibodies are approved for clinical use as listed in the FDA-approved list of biologics. In addition to potential therapeutic effects, such antibodies can also be used for diagnosis when bound to MBs or other reporters. By coupling the specificity of antibodies with BBBD, targeted theranostics represent a non-invasive means of cost-effectively diagnosing and treating pathologies beyond the BBB. A demonstration of such bimodal application is the treatment is MB+FUS BBBD Alzheimer's disease (AD) therapy. Conventional diagnosis of AD begins with an implicative approach, by way of behavioral symptoms and family history, and no physiological test short of a post-mortem biopsy is able to identify positively AD pathologies. Due to the ability to overcome the physical barrier of CNS vasculature, MB+FUS is capable of accessing the parenchyma in which AD-specific plaques and biomarkers are present [96–99]. In 2008, Raymond et al. demonstrated that MB+FUS BBBD followed by an injection of amyloid-targeted antibodies (anti-Aβ) localized in brain tissue with high amyloid loads [96].

Two categories of diseases have been of particular interest for MB+FUS BBBD studies: neurodegenerative diseases and cancer. Brain cancer therapy is an understandably attractive target for MB+FUS BBBD, due to the systemic effects of chemotherapeutic agent, the desire to reduce dose and increase therapeutic index, and the invasive nature of re-introducing chemotherapeutic agent via intracranial surgery. A handful of groups have shown improved chemotherapeutic delivery to the brain using MB+FUS in rodent models [100–102]; a functional improvement in glioblastoma mouse models was shown by Kovacs et al. in 2014 [103]. Doxorubicin, co-injected microbubbles were stimulated in GL261 brain tumors with 612.5 kHz at 0.4 MPa (PRP, PNP unspecified). While mice treated with only doxorubicin or FUS demonstrated identical median survival times of 22 days, MB+FUS with doxorubicin-treated mice demonstrated an impressive 66% improvement in survival time of 37 days. Other studies have examined the benefits of augmenting emerging cancer therapy methods such as boron neutron capture therapy with MB+FUS, by delivering *p*-boronophenylalanine (BPA), a molecule exhibiting selective uptake by malignant cells, and subsequent destruction of nearby (5-9 μm) tissue through localized radiation from neutron capture. Using MB+FUS BBBD, Alkins et al. demonstrated a three-fold uptake in 9L rat gliosarcoma models using 558 kHz, 0.4 MPa after injection of BPA and Definity

[104]. Similarly, Yang et al. demonstrated that application of MB+FUS resulted in 3.6 times the BPA concentration in F98 glioma tumors at 1 MHz at an undisclosed acoustic pressure after injection of Sonovue and BPA in adolescent rats [105]. Neither studies reported the presence of tissue damage after histological staining.

While MB+FUS provides a significant improvement in drug localization for chemotherapeutic agents, drugs such as 1-3-bis(2-chloroethyl)-1-nitrosourea (BCNU) are relatively small and pass through the BBB without MB+FUS. However, a well-studied therapeutic agent for Alzheimer's disease, anti-Aβ, only passes through the BBB at very low rates [106]. To be effective, immunotherapy requires antibodies such as anti-Aβ to pass through the BBB and "label" diseased tissue for T-cell mediated clearance [107]. Burgess et al. demonstrated a task completion improvement of 72% in rat models of Alzheimer's in memory studies, similar to that of healthy mice, using Definity (*FVD* = 0.02 mL/kg) stimulated with 1.68 MHz, 1.2 MPa PNP over a 2-min duration. Histology revealed an increase in learning-associated DCX-positive neurons, as well as a 332% increase in dendrite length in treated populations.

Gene therapy without MB+FUS shares similar challenges with immunotherapy: namely, the BBB poses a significant barrier to efficient viral localization in the parenchyma. As of the time of this writing, no biodegradable non-viral agents have been able to induce transfection of neuronal tissue *in vivo* with MB+FUS. On the other hand, modified viral particles have been shown to induce robust transduction in neurons, and at least six studies have demonstrated successful transduction of neurons using adeno-associated virus (AAV) [108–112,14].

Summary and outlook

MB+FUS BBBD promises unprecedented advantages over existing intracranial drug delivery methods, as well as a significant number of tunable parameters that affect its safety and efficiency. Numerous studies have been published on the effect of acoustic parameters, oftentimes highlighting the feasibility of novel methodological and analytical techniques; fewer studies have isolated the effect of the microbubbles themselves, and even fewer have focused on biochemical, immunological and physiological parameters. However, optimization of MB+FUS BBBD, and efforts to improve its clinical relevance, are well underway; its safety and efficiency have been demonstrated in several animal models with a wide range of payloads, and interactions between parameters are being explored to provide new avenues of optimization.

Nonetheless, standardization of MB+FUS parameters and implementation of rigorous safety metrics are essential to improving our understanding of its effects and eventual clinical translation. Challenging this goal are the numerous permutations of microbubble, ultrasound and physiological parameters. Specifically, readily varied parameters such as FUS frequency and amplitude have been extensively studied, but the lack of optimized and commonly shared parameters in microbubble formulations, dosage metrics, animal models, as well as histological and behavior assays for safety have stymied productive overlap in past studies. While unified parameters, such as mechanical index (*MI*) and microbubble volume dose (*MVD*), incorporate multiple individual parameters into single reference parameters that may be more suitable for standardization, optimization of such parameters and others, as well as deeper characterization of their tissue- and cell-level effects, remain yet to be completed. Finally, MB+FUS BBBD is a highly translational field of study, and widely accepted measures of safety should be adopted from well-established disciplines to accelerate collaboration and improve understanding and clinical relevance.

Abbreviations

AAV: adeno-associated virus; AD: Alzheimer's disease; BBB: blood-brain-barrier; BBBD: blood-brain-barrier disruption; BCNU: bis-chloroethylnitrosourea; BPA: *p*-boronophenylalanine; CED: convection-enhanced delivery; CCTFs: cytokines, chemokines and trophic factors; CNS: central nervous system; DCX: doublecortin; EPR: enhanced permeability and retention; FDA: US Food and Drug Administration; FVD: fluid volume dose; GDNF: glial cell-line derived neurotropic factor; HIFU: high-intensity focused ultrasound; HIV: human immunodeficiency virus; Hsp: heat shock protein; Iba1: ionized calcium-binding adapter molecule 1; MB: microbubble; MB+FUS: microbubble-assisted focused-ultrasound; MI: mechanical index; MND: microbubble number dose; MRI: magnetic resonance imaging; MRIg-FUS: MRI-guided focused ultrasound; MVD: microbubble volume dose; NFκB: nuclear factor kappa-light-chain-enhancer of activated B cells; PCD: passive cavitation device; PNP: peak negative pressure; PRF: pulse repetition frequency; PSD: particle size distribution; SIR: sterile immune response; TNFα: tumor necrosis factor alpha; UCA: ultrasound contrast agents.

Competing Interests

The authors have declared that no competing interest exists.

References

1. World Health Organization, editor. Neurological disorders: public health challenges. Geneva: World Health Organization; 2006. 218 p.
2. Chien L-N, Gittleman H, Ostrom QT, Hung K-S, Sloan AE, Hsieh Y-C, Kruchko C, Rogers LR, Wang Y-FG, Chiou H-Y, Barnholtz-Sloan JS. Comparative Brain and Central Nervous System Tumor Incidence and Survival between the United States and Taiwan Based on Population-Based Registry. Front Public Health [Internet]. 2016 Jul 21 [cited 2018 Feb 7];4. Available from: https://www.ncbi.nlm.nih.gov/pmc/articles/PMC4954825/
3. Ostrom QT, Gittleman H, Xu J, Kromer C, Wolinsky Y, Kruchko C, Barnholtz-Sloan JS. CBTRUS Statistical Report: Primary Brain and Other Central Nervous System Tumors Diagnosed in the United States in 2009–2013. Neuro-Oncol. 2016 Oct;18(suppl_5):v1–75.
4. Scheld WM. Drug delivery to the central nervous system: general principles and relevance to therapy for infections of the central nervous system. Rev Infect Dis. 1989 Dec;11 Suppl 7:S1669-1690.
5. Little RC. Physiology of the heart and circulation. 3rd ed. Chicago: Year Book Medical Publishers; 1985. 359 p.
6. Pardridge WM. The blood-brain barrier: bottleneck in brain drug development. NeuroRx. 2005;2(1):3–14.
7. Löscher W, Potschka H. Drug resistance in brain diseases and the role of drug efflux transporters. Nat Rev Neurosci. 2005 Aug;6(8):591–602.
8. Deeken JF, Loscher W. The Blood-Brain Barrier and Cancer: Transporters, Treatment, and Trojan Horses. Clin Cancer Res. 2007 Mar 15;13(6):1663–74.
9. Barth RF, Yang W, Rotaru JH, Moeschberger ML, Joel DD, Nawrocky MM, Goodman JH, Soloway AH. Boron neutron capture therapy of brain tumors: enhanced survival following intracarotid injection of either sodium borocaptate or boronophenylalanine with or without blood-brain barrier disruption. Cancer Res. 1997 Mar 15;57(6):1129–36.
10. Pardridge WM, Boado RJ. Reengineering biopharmaceuticals for targeted delivery across the blood-brain barrier. Methods Enzymol. 2012;503:269–92.
11. Marquet F, Tung Y-S, Teichert T, Ferrera VP, Konofagou EE. Noninvasive, Transient and Selective Blood-Brain Barrier Opening in Non-Human Primates In Vivo. Brechbiel MW, editor. PLoS ONE. 2011 Jul 22;6(7):e22598.
12. McDannold N, Vykhodtseva N, Raymond S, Jolesz FA, Hynynen K. MRI-guided targeted blood-brain barrier disruption with focused ultrasound: histological findings in rabbits. Ultrasound Med Biol. 2005 Nov;31(11):1527–37.
13. Choi JJ, Wang S, Tung Y-S, Morrison B, Konofagou EE. Molecules of Various Pharmacologically-Relevant Sizes Can Cross the Ultrasound-Induced Blood-Brain Barrier Opening in vivo. Ultrasound Med Biol. 2010 Jan;36(1):58–67.
14. Song K-H, Fan AC, Hinkle JJ, Newman J, Borden MA, Harvey BK. Microbubble gas volume: A unifying dose parameter in blood-brain barrier opening by focused ultrasound. Theranostics. 2017;7(1):144–52.
15. Errico C, Pierre J, Pezet S, Desailly Y, Lenkei Z, Couture O, Tanter M. Ultrafast ultrasound localization microscopy for deep super-resolution vascular imaging. Nature. 2015 Nov 25;527(7579):499–502.
16. O'Reilly MA, Hynynen K. Blood-Brain Barrier: Real-time Feedback-controlled Focused Ultrasound Disruption by Using an Acoustic Emissions–based Controller. Radiology. 2012 Apr;263(1):96–106.
17. Sun T, Zhang Y, Power C, Alexander PM, Sutton JT, Aryal M, Vykhodtseva N, Miller EL, McDannold NJ. Closed-loop control of targeted ultrasound drug delivery across the blood–brain/tumor barriers in a rat glioma model. Proc Natl Acad Sci. 2017 Nov 28;114(48):E10281–90.
18. Kamimura HA, Flament J, Valette J, Cafarelli A, Aron Badin R, Hantraye P, Larrat B. Feedback control of microbubble cavitation for ultrasound-mediated blood-brain barrier disruption in non-human primates under magnetic resonance guidance. J Cereb Blood Flow Metab. 2018 Jan 1;271678X17753514.
19. Ellegala DB. Imaging Tumor Angiogenesis With Contrast Ultrasound and Microbubbles Targeted to v 3. Circulation. 2003 Jul 22;108(3):336–41.
20. Borden MA, Caskey CF, Little E, Gillies RJ, Ferrara KW. DNA and Polylysine Adsorption and Multilayer Construction onto Cationic Lipid-Coated Microbubbles. Langmuir. 2007 Aug;23(18):9401–8.
21. Chen CC, Borden MA. Ligand Conjugation to Bimodal Poly(ethylene glycol) Brush Layers on Microbubbles. Langmuir. 2010 Aug 17;26(16):13183–94.
22. Konofagou EE, Tung Y-S, Choi J, Deffieux T, Baseri B, Vlachos F. Ultrasound-Induced Blood-Brain Barrier Opening. Curr Pharm Biotechnol. 2012 Jun;13(7):1332–45.
23. Cline HE, Hynynen K, Hardy CJ, Watkins RD, Schenck JF, Jolesz FA. MR temperature mapping of focused ultrasound surgery. Magn Reson Med. 1994 Jun;31(6):628–36.
24. Hynynen K, McDannold N, Vykhodtseva N, Jolesz FA. Noninvasive MR imaging-guided focal opening of the blood-brain barrier in rabbits. Radiology. 2001 Sep;220(3):640–6.
25. Zhou Y. Dynamics of Sonoporation Correlated with Acoustic Cavitation Activities. [cited 2012 Aug 21]; Available from: http://ukpmc.ac.uk/articles/PMC2267145/pdf/L51.pdf
26. Hwang JH, Tu J, Brayman AA, Matula TJ, Crum LA. Correlation between inertial cavitation dose and endothelial cell damage in vivo. Ultrasound Med Biol. 2006 Oct;32(10):1611–9.
27. Johnsen E, Warnez M. Tissue damage produced by cavitation: The role of viscoelasticity. J Acoust Soc Am. 2014 Oct;136(4):2280–2280.
28. Cramer HC, Estrada JB, Scimone MT, Franck C. Inertial Microcavitation as a Neural Cell Damage Mechanism in a 3D In Vitro Model of Blast Traumatic Brain Injury. Biophys J. 2018 Feb;114(3):518a.
29. Chen H, Brayman AA, Bailey MR, Matula TJ. Blood vessel rupture by cavitation. Urol Res. 2010 Aug;38(4):321–6.
30. Chen H, Brayman AA, Kreider W, Bailey MR, Matula TJ. Observations of translation and jetting of ultrasound-activated microbubbles in mesenteric microvessels. Ultrasound Med Biol. 2011 Dec;37(12):2139–48.
31. Chen H, Brayman AA, Evan AP, Matula TJ. Preliminary observations on the spatial correlation between short-burst microbubble oscillations and vascular bioeffects. Ultrasound Med Biol. 2012 Dec;38(12):2151–62.
32. Song K-H, Fan AC, Brlansky JT, Trudeau T, Gutierrez-Hartmann A, Calvisi ML, Borden MA. High Efficiency Molecular Delivery with Sequential Low-Energy Sonoporation Bursts. Theranostics. 2015;5(12):1419–27.
33. Tung Y-S, Vlachos F, Feshitan JA, Borden MA, Konofagou EE. The mechanism of interaction between focused ultrasound and microbubbles in blood-brain barrier opening in mice. J Acoust Soc Am. 2011 Nov;130(5):3059–67.
34. Chen H, Konofagou EE. The size of blood-brain barrier opening induced by focused ultrasound is dictated by the acoustic pressure. J Cereb Blood Flow Metab Off J Int Soc Cereb Blood Flow Metab. 2014 Jul;34(7):1197–204.
35. Aryal M, Fischer K, Gentile C, Gitto S, Zhang Y-Z, McDannold N. Effects on P-Glycoprotein Expression after Blood-Brain Barrier Disruption Using Focused Ultrasound and Microbubbles. Toborek M, editor. PLOS ONE. 2017 Jan 3;12(1):e0166061.
36. Cho H, Lee H-Y, Han M, Choi J, Ahn S, Lee T, Chang Y, Park J. Localized Down-regulation of P-glycoprotein by Focused Ultrasound and Microbubbles induced Blood-Brain Barrier Disruption in Rat Brain. Sci Rep [Internet]. 2016 Nov [cited 2018 Jun 5];6(1). Available from: http://www.nature.com/articles/srep31201
37. Wong AD, Ye M, Levy AF, Rothstein JD, Bergles DE, Searson PC. The blood-brain barrier: an engineering perspective. Front Neuroengineering [Internet]. 2013 Aug 30 [cited 2018 Mar 5];6. Available from: https://www.ncbi.nlm.nih.gov/pmc/articles/PMC3757302/
38. Wolak DJ, Thorne RG. Diffusion of Macromolecules in the Brain: Implications for Drug Delivery. Mol Pharm. 2013 May 6;10(5):1492–504.
39. Thorne RG, Hrabětová S, Nicholson C. Diffusion of Epidermal Growth Factor in Rat Brain Extracellular Space Measured by Integrative Optical Imaging. J Neurophysiol. 2004 Dec;92(6):3471–81.
40. Garbayo E, Ansorena E, Lana H, Carmona-Abellan M del M, Marcilla I, Lanciego JL, Luquin MR, Blanco-Prieto MJ. Brain delivery of microencapsulated GDNF induces functional and structural recovery in parkinsonian monkeys. Biomaterials. 2016 Dec;110:11–23.
41. Goertz DE, de Jong N, van der Steen AFW. Attenuation and Size Distribution Measurements of Definity™ and Manipulated Definity™ Populations. Ultrasound Med Biol. 2007 Sep;33(9):1376–88.
42. Wang S, Samiotaki G, Olumolade O, Feshitan JA, Konofagou EE. Microbubble Type and Distribution Dependence of Focused Ultrasound-Induced Blood–Brain Barrier Opening. Ultrasound Med Biol. 2014 Jan;40(1):130–7.
43. Silburt J, Lipsman N, Aubert I. Disrupting the blood–brain barrier with focused ultrasound: Perspectives on inflammation and regeneration. Proc Natl Acad Sci. 2017 Aug 15;114(33):E6735–6.
44. Kovacs ZI, Burks SR, Frank JA. Reply to Silburt et al.: Concerning sterile inflammation following focused ultrasound and microbubbles in the brain. Proc Natl Acad Sci. 2017 Aug 15;114(33):E6737–8.
45. McMahon D, Hynynen K. Acute Inflammatory Response Following Increased Blood-Brain Barrier Permeability Induced by Focused Ultrasound is Dependent on Microbubble Dose. Theranostics. 2017;7(16):3989–4000.
46. Kovacs ZI, Burks SR, Frank JA. Focused ultrasound with microbubbles induces sterile inflammatory response proportional to the blood brain barrier opening: Attention to experimental conditions. Theranostics. 2018;8(8):2245–8.
47. Wu S-K, Chu P-C, Chai W-Y, Kang S-T, Tsai C-H, Fan C-H, Yeh C-K, Liu H-L. Characterization of Different Microbubbles in Assisting Focused Ultrasound-Induced Blood-Brain Barrier Opening. Sci Rep. 2017 Apr 20;7:46689.
48. Koch S, Pohl P, Cobet U, Rainov NG. Ultrasound enhancement of liposome-mediated cell transfection is caused by cavitation effects. Ultrasound Med Biol. 2000;26(5):897–903.
49. Miller DL, Bao S, Morris JE. Sonoporation of cultured cells in the rotating tube exposure system. Ultrasound Med Biol. 1999;25(1):143–149.
50. Kovacs ZI, Kim S, Jikaria N, Qureshi F, Milo B, Lewis BK, Bresler M, Burks SR, Frank JA. Disrupting the blood–brain barrier by focused ultrasound induces sterile inflammation. Proc Natl Acad Sci U S A. 2017 Jan 3;114(1):E75–84.
51. Choi JJ, Feshitan JA, Baseri B, Shougang Wang, Yao-Sheng Tung, Borden MA, Konofagou EE. Microbubble-Size Dependence of Focused Ultrasound-Induced Blood-Brain Barrier Opening in Mice In Vivo. IEEE Trans Biomed Eng. 2010 Jan;57(1):145–54.

52. Sirsi S, Feshitan J, Kwan J, Homma S, Borden M. Effect of microbubble size on fundamental mode high frequency ultrasound imaging in mice. Ultrasound Med Biol. 2010;36(6):935–948.
53. Samiotaki G, Vlachos F, Tung Y-S, Konofagou EE. A quantitative pressure and microbubble-size dependence study of focused ultrasound-induced blood-brain barrier opening reversibility in vivo using MRI. Magn Reson Med. 2012 Mar;67(3):769–77.
54. Sennoga CA, Yeh JSM, Alter J, Stride E, Nihoyannopoulos P, Seddon JM, Haskard DO, Hajnal JV, Tang M-X, Eckersley RJ. Evaluation of methods for sizing and counting of ultrasound contrast agents. Ultrasound Med Biol. 2012 May;38(5):834–45.
55. Satinover SJ, Dove JD, Borden MA. Single-particle optical sizing of microbubbles. Ultrasound Med Biol. 2014 Jan;40(1):138–47.
56. Sarkar K, Katiyar A, Jain P. Growth and dissolution of an encapsulated contrast microbubble: effects of encapsulation permeability. Ultrasound Med Biol. 2009;35(8):1385.
57. O'Reilly MA, Waspe AC, Ganguly M, Hynynen K. Focused-Ultrasound Disruption of the Blood-Brain Barrier Using Closely-Timed Short Pulses: Influence of Sonication Parameters and Injection Rate. Ultrasound Med Biol. 2011 Apr;37(4):587–94.
58. Garg S, Thomas AA, Borden MA. The effect of lipid monolayer in-plane rigidity on in vivo microbubble circulation persistence. Biomaterials. 2013 Sep;34(28):6862–70.
59. Kabalnov A, Klein D, Pelura T, Schutt E, Weers J. Dissolution of multicomponent microbubbles in the bloodstream: 1. theory. Ultrasound Med Biol. 1998 Jun 1;24(5):739–49.
60. Ferrara K, Pollard R, Borden M. Ultrasound microbubble contrast agents: fundamentals and application to gene and drug delivery. Annu Rev Biomed Eng. 2007;9:415–47.
61. Åslund AKO, Berg S, Hak S, Mørch Ý, Torp SH, Sandvig A, Widerøe M, Hansen R, de Lange Davies C. Nanoparticle delivery to the brain--By focused ultrasound and self-assembled nanoparticle-stabilized microbubbles. J Control Release Off J Control Release Soc. 2015 Dec 28;220(Pt A):287–94.
62. Åslund AKO, Snipstad S, Healey A, Kvåle S, Torp SH, Sontum PC, Davies C de L, van Wamel A. Efficient Enhancement of Blood-Brain Barrier Permeability Using Acoustic Cluster Therapy (ACT). Theranostics. 2017;7(1):23–30.
63. Burke CW, Alexander E, Timbie K, Kilbanov AL, Price RJ. Ultrasound-activated agents comprised of 5FU-bearing nanoparticles bonded to microbubbles inhibit solid tumor growth and improve survival. Mol Ther J Am Soc Gene Ther. 2014 Feb;22(2):321–8.
64. Azhari H. Basics of Biomedical Ultrasound for Engineers. John Wiley & Sons; 2010. 395 p.
65. Azhari H. Appendix A: Typical Acoustic Properties of Tissues. In: Basics of Biomedical Ultrasound for Engineers [Internet]. John Wiley & Sons, Inc.; 2010 [cited 2018 Feb 19]. p. 313–4. Available from: http://onlinelibrary.wiley.com/doi/10.1002/9780470561478.app1/summary
66. Pichardo S, Sin VW, Hynynen K. Multi-frequency characterization of the speed of sound and attenuation coefficient for longitudinal transmission of freshly excised human skulls. Phys Med Biol. 2011 Jan 7;56(1):219–50.
67. O'Reilly MA, Muller A, Hynynen K. Ultrasound Insertion Loss of Rat Parietal Bone Appears to Be Proportional to Animal Mass at Submegahertz Frequencies. Ultrasound Med Biol. 2011 Nov;37(11):1930–7.
68. McDannold N, Arvanitis CD, Vykhodtseva N, Livingstone MS. Blood-brain barrier disruption in nonhuman primates using a clinical MRI-guided focused ultrasound system: preliminary results. In 2010.
69. Tung Y-S, Marquet F, Teichert T, Ferrera V, Konofagou EE. Feasibility of noninvasive cavitation-guided blood-brain barrier opening using focused ultrasound and microbubbles in nonhuman primates. Appl Phys Lett. 2011;98(16):163704.
70. McDannold N, Arvanitis CD, Vykhodtseva N, Livingstone MS. Temporary disruption of the blood-brain barrier by use of ultrasound and microbubbles: safety and efficacy evaluation in rhesus macaques. Cancer Res. 2012 Jul 15;72(14):3652–63.
71. Sheikov N, McDannold N, Jolesz F, Zhang Y-Z, Tam K, Hynynen K. Brain arterioles show more active vesicular transport of blood-borne tracer molecules than capillaries and venules after focused ultrasound-evoked opening of the blood-brain barrier. Ultrasound Med Biol. 2006 Sep;32(9):1399–409.
72. Hassan M, Barrefelt A, Saghafian M, Kuiper R, Ye F, Egri G, Klickermann M, Brismar TB, Aspelin P, Muhammed M, Dähne L. Biodistribution, kinetics, and biological fate of SPION microbubbles in the rat. Int J Nanomedicine. 2013 Aug;3241-54.
73. Sembulingam K, Sembulingam P. Essentials of medical physiology. 2013.
74. McDannold N, Zhang Y, Vykhodtseva N. The Effects of Oxygen on Ultrasound-Induced Blood–Brain Barrier Disruption in Mice. Ultrasound Med Biol. 2017 Feb;43(2):469–75.
75. Barnard RJ, Corre K, Cho H. Effect of training on the resting heart rate of rats. Eur J Appl Physiol. 1976 Sep 23;35(4):285–9.
76. Lynn JG, Zwemer RL, Chick AJ, Miller AE. A NEW METHOD FOR THE GENERATION AND USE OF FOCUSED ULTRASOUND IN EXPERIMENTAL BIOLOGY. J Gen Physiol. 1942 Nov 20;26(2):179–93.
77. Bakay L, Ballantine HT, Hueter TF, Sosa D. Ultrasonically produced changes in the blood-brain barrier. AMA Arch Neurol Psychiatry. 1956 Nov;76(5):457–67.
78. Hynynen K, Freund W, Cline H, Chung A, Watkins R, Vetro J, Jolesz F. A clinical, noninvasive, MR imaging-monitored ultrasound surgery method. RadioGraphics. 1996 Jan;16(1):185–95.
79. Choi JJ, Pernot M, Small SA, Konofagou EE. Noninvasive, transcranial and localized opening of the blood-brain barrier using focused ultrasound in mice. Ultrasound Med Biol. 2007 Jan;33(1):95–104.
80. Chu P-C, Chai W-Y, Tsai C-H, Kang S-T, Yeh C-K, Liu H-L. Focused Ultrasound-Induced Blood-Brain Barrier Opening: Association with Mechanical Index and Cavitation Index Analyzed by Dynamic Contrast-Enhanced Magnetic-Resonance Imaging. Sci Rep [Internet]. 2016 Dec [cited 2018 Mar 27];6(1). Available from: http://www.nature.com/articles/srep33264
81. Liu H-L, Wai Y-Y, Chen W-S, Chen J-C, Hsu P-H, Wu X-Y, Huang W-C, Yen T-C, Wang J-J. Hemorrhage Detection During Focused-Ultrasound Induced Blood-Brain-Barrier Opening by Using Susceptibility-Weighted Magnetic Resonance Imaging. Ultrasound Med Biol. 2008 Apr;34(4):598–606.
82. McDannold N, Vykhodtseva N, Hynynen K. Effects of Acoustic Parameters and Ultrasound Contrast Agent Dose on Focused-Ultrasound Induced Blood-Brain Barrier Disruption. Ultrasound Med Biol. 2008 Jun;34(6):930–7.
83. Wu S-Y, Tung Y-S, Marquet F, Downs ME, Sanchez CS, Chen CC, Ferrera V, Konofagou E. Transcranial cavitation detection in primates during blood-brain barrier opening-a performance assessment study. IEEE Trans Ultrason Ferroelectr Freq Control. 2014 Jun;61(6):966–78.
84. Reinhard M, Hetzel A, Kruger S, Kretzer S, Talazko J, Ziyeh S, Weber J, Els T. Blood-Brain Barrier Disruption By Low-Frequency Ultrasound. Stroke. 2006 Jun 1;37(6):1546–8.
85. Gerriets T, Walberer M, Nedelmann M, Bachmann G, Kaps M. Blood-Brain Barrier Disruption by Low-Frequency Ultrasound. Stroke. 2007 Feb 1;38(2):251–251.
86. Doinikov AA, Haac JF, Dayton PA. Resonance frequencies of lipid-shelled microbubbles in the regime of nonlinear oscillations. Ultrasonics. 2009;49(2):263–268.
87. Meer SM van der, Dollet B, Voormolen MM, Chin CT, Bouakaz A, Jong N de, Versluis M, Lohse D. Microbubble spectroscopy of ultrasound contrast agents. J Acoust Soc Am. 2007 Jan 1;121(1):648–56.
88. Chen H, Konofagou EE. The Size of Blood–Brain Barrier Opening Induced by Focused Ultrasound is Dictated by the Acoustic Pressure. J Cereb Blood Flow Metab. 2014 Jul;34(7):1197–204.
89. Choi JJ, Selert K, Gao Z, Samiotaki G, Baseri B, Konofagou EE. Noninvasive and localized blood-brain barrier disruption using focused ultrasound can be achieved at short pulse lengths and low pulse repetition frequencies. J Cereb Blood Flow Metab Off J Int Soc Cereb Blood Flow Metab. 2011 Feb;31(2):725–37.
90. Downs ME, Buch A, Sierra C, Karakatsani ME, Chen S, Konofagou EE, Ferrera VP. Long-term safety of repeated blood-brain barrier opening via focused ultrasound with microbubbles in non-human primates performing a cognitive task. PloS One. 2015;10(5):e0125911.
91. Aronowski J, Zhao X. Molecular Pathophysiology of Cerebral Hemorrhage: Secondary Brain Injury. Stroke. 2011 Jun 1;42(6):1781–6.
92. McMahon D, Hynynen K. Reply to Kovacs *et al* .: Concerning acute inflammatory response following focused ultrasound and microbubbles in the brain. Theranostics. 2018;8(8):2249–50.
93. Liu H-L, Hua M-Y, Yang H-W, Huang C-Y, Chu P-C, Wu J-S, Tseng I-C, Wang J-J, Yen T-C, Chen P-Y, Wei K-C. Magnetic resonance monitoring of focused ultrasound/magnetic nanoparticle targeting delivery of therapeutic agents to the brain. Proc Natl Acad Sci. 2010 Aug 24;107(34):15205–10.
94. Lipsman N, Ironside S, Alkins R, Bethune A, Huang Y, Perry J, Sahgal A, Trudeau M, Hynynen K, Mainprize T. ACTR-42. INITIAL EXPERIENCE OF BLOOD-BRAIN BARRIER OPENING FOR CHEMOTHERAPEUTIC-DRUG DELIVERY TO BRAIN TUMOURS BY MR-GUIDED FOCUSED ULTRASOUND. Neuro-Oncol. 2017 Nov 6;19(suppl_6):vi9–vi9.
95. Carpentier A, Canney M, Vignot A, Reina V, Beccaria K, Horodyckid C, Karachi C, Leclercq D, Lafon C, Chapelon J-Y, Capelle L, Cornu P, Sanson M, Hoang-Xuan K, Delattre J-Y, Idbaih A. Clinical trial of blood-brain barrier disruption by pulsed ultrasound. Sci Transl Med. 2016 Jun 15;8(343):343re2-343re2.
96. Raymond SB, Treat LH, Dewey JD, McDannold NJ, Hynynen K, Bacskai BJ. Ultrasound Enhanced Delivery of Molecular Imaging and Therapeutic Agents in Alzheimer's Disease Mouse Models. PLoS ONE [Internet]. 2008 May 14 [cited 2017 Dec 21];3(5). Available from: https://www.ncbi.nlm.nih.gov/pmc/articles/PMC2364662/
97. Choi JJ, Wang S, Brown TR, Small SA, Duff KE, Konofagou EE. Noninvasive and transient blood-brain barrier opening in the hippocampus of Alzheimer's double transgenic mice using focused ultrasound. Ultrason Imaging. 2008;30(3):189–200.
98. Jordão JF, Ayala-Grosso CA, Markham K, Huang Y, Chopra R, McLaurin J, Hynynen K, Aubert I. Antibodies Targeted to the Brain with Image-Guided Focused Ultrasound Reduces Amyloid-β Plaque Load in the TgCRND8 Mouse Model of Alzheimer's Disease. PLoS ONE [Internet]. 2010 May 11 [cited 2017 Dec 21];5(5). Available from: https://www.ncbi.nlm.nih.gov/pmc/articles/PMC2868024/
99. Burgess A, Dubey S, Yeung S, Hough O, Eterman N, Aubert I, Hynynen K. Alzheimer disease in a mouse model: MR imaging–guided focused ultrasound targeted to the hippocampus opens the blood-brain barrier and improves pathologic abnormalities and behavior. Radiology. 2014;273(3):736–745.

100. Treat LH, McDannold N, Vykhodtseva N, Zhang Y, Tam K, Hynynen K. Targeted delivery of doxorubicin to the rat brain at therapeutic levels using MRI-guided focused ultrasound. Int J Cancer. 2007 Aug 15;121(4):901–7.
101. Aryal M, Park J, Vykhodtseva N, Zhang Y-Z, McDannold N. Enhancement in blood-tumor barrier permeability and delivery of liposomal doxorubicin using focused ultrasound and microbubbles: evaluation during tumor progression in a rat glioma model. Phys Med Biol. 2015 Mar 21;60(6):2511–27.
102. Aryal M, Vykhodtseva N, Zhang Y-Z, McDannold N. Multiple sessions of liposomal doxorubicin delivery via focused ultrasound mediated blood–brain barrier disruption: A safety study. J Controlled Release. 2015 Apr;204:60–9.
103. Kovacs Z, Werner B, Rassi A, Sass JO, Martin-Fiori E, Bernasconi M. Prolonged survival upon ultrasound-enhanced doxorubicin delivery in two syngenic glioblastoma mouse models. J Controlled Release. 2014 Aug;187:74–82.
104. Alkins RD, Brodersen PM, Sodhi RNS, Hynynen K. Enhancing drug delivery for boron neutron capture therapy of brain tumors with focused ultrasound. Neuro-Oncol. 2013 Sep;15(9):1225–35.
105. Yang F-Y, Lin Y-L, Chou F-I, Lin Y-C, Hsueh Liu Y-W, Chang L-W, Hsieh Y-L. Pharmacokinetics of BPA in Gliomas with Ultrasound Induced Blood-Brain Barrier Disruption as Measured by Microdialysis. Coles JA, editor. PLoS ONE. 2014 Jun 17;9(6):e100104.
106. Banks WA, Terrell B, Farr SA, Robinson SM, Nonaka N, Morley JE. Passage of amyloid beta protein antibody across the blood-brain barrier in a mouse model of Alzheimer's disease. Peptides. 2002 Dec;23(12):2223–6.
107. Wilcock DM, Colton CA. Anti-amyloid-beta immunotherapy in Alzheimer's disease: relevance of transgenic mouse studies to clinical trials. J Alzheimers Dis JAD. 2008 Dec;15(4):555–69.
108. Thévenot E, Jordão JF, O'Reilly MA, Markham K, Weng Y-Q, Foust KD, Kaspar BK, Hynynen K, Aubert I. Targeted delivery of self-complementary adeno-associated virus serotype 9 to the brain, using magnetic resonance imaging-guided focused ultrasound. Hum Gene Ther. 2012 Nov;23(11):1144–55.
109. Hsu P-H, Wei K-C, Huang C-Y, Wen C-J, Yen T-C, Liu C-L, Lin Y-T, Chen J-C, Shen C-R, Liu H-L. Noninvasive and targeted gene delivery into the brain using microbubble-facilitated focused ultrasound. PloS One. 2013;8(2):e57682.
110. Alonso A, Reinz E, Leuchs B, Kleinschmidt J, Fatar M, Geers B, Lentacker I, Hennerici MG, de Smedt SC, Meairs S. Focal Delivery of AAV2/1-transgenes Into the Rat Brain by Localized Ultrasound-induced BBB Opening. Mol Ther Nucleic Acids. 2013;2:e73.
111. Wang S, Olumolade OO, Sun T, Samiotaki G, Konofagou EE. Noninvasive, neuron-specific gene therapy can be facilitated by focused ultrasound and recombinant adeno-associated virus. Gene Ther. 2015;22(1):104–110.
112. Wang S, Karakatsani ME, Fung C, Sun T, Acosta C, Konofagou E. Direct brain infusion can be enhanced with focused ultrasound and microbubbles. J Cereb Blood Flow Metab. 2017 Feb;37(2):706–14.
113. Hyvelin J-M, Gaud E, Costa M, Helbert A, Bussat P, Bettinger T, Frinking P. Characteristics and Echogenicity of Clinical Ultrasound Contrast Agents: An In Vitro and In Vivo Comparison Study. J Ultrasound Med. 2017 May 1;36(5):941–53.
114. Ting C-Y, Fan C-H, Liu H-L, Huang C-Y, Hsieh H-Y, Yen T-C, Wei K-C, Yeh C-K. Concurrent blood–brain barrier opening and local drug delivery using drug-carrying microbubbles and focused ultrasound for brain glioma treatment. Biomaterials. 2012 Jan;33(2):704–12.
115. Fan C-H, Liu H-L, Ting C-Y, Lee Y-H, Huang C-Y, Ma Y-J, Wei K-C, Yen T-C, Yeh C-K. Submicron-Bubble-Enhanced Focused Ultrasound for Blood–Brain Barrier Disruption and Improved CNS Drug Delivery. Shohet RV, editor. PLoS ONE. 2014 May 2;9(5):e96327.
116. Yang F-Y, Chen Y-W, Chou F-I, Yen S-H, Lin Y-L, Wong T-T. Boron neutron capture therapy for glioblastoma multiforme: enhanced drug delivery and antitumor effect following blood–brain barrier disruption induced by focused ultrasound. Future Oncol. 2012 Oct;8(10):1361–9.
117. Treat LH, McDannold N, Zhang Y, Vykhodtseva N, Hynynen K. Improved Anti-Tumor Effect of Liposomal Doxorubicin After Targeted Blood-Brain Barrier Disruption by MRI-Guided Focused Ultrasound in Rat Glioma. Ultrasound Med Biol. 2012 Oct;38(10):1716–25.
118. Wang X, Guo S, Lu S, Zhou J, Li J, Xia S. Ultrasound-induced release of GDNF from lipid coated microbubbles injected into striatum reduces hypoxic–ischemic injury in neonatal rats. Brain Res Bull. 2012 Aug;88(5):495–500.
119. Wang X, Cui G, Yang X, Zhang Z, Shi H, Zu J, Hua F, Shen X. Intracerebral administration of ultrasound-induced dissolution of lipid-coated GDNF microbubbles provides neuroprotection in a rat model of Parkinson's disease. Brain Res Bull. 2014 Apr;103:60–5.
120. Kinoshita M, Yoshioka Y, Okita Y, Hashimoto N, Yoshimine T. MR molecular imaging of HER-2 in a murine tumor xenograft by SPIO labeling of anti-HER-2 affibody. Contrast Media Mol Imaging. 2010;n/a-n/a.
121. Burgess A, Huang Y, Querbes W, Sah DW, Hynynen K. Focused ultrasound for targeted delivery of siRNA and efficient knockdown of Htt expression. J Controlled Release. 2012 Oct;163(2):125–9.
122. Burgess A, Huang Y, Querbes W, Sah DW, Hynynen K. Non-invasive delivery of small interfering rubonucleic acid for reduction of Huntingtin expression in the brain is achieved using focused ultrasound to disrupt the blood-brain barrier. Proc Meet Acoust. 2013;19(1):075057.
123. Wu F, Wang Z-B, Chen W-Z, Zhu H, Bai J, Zou J-Z, Li K-Q, Jin C-B, Xie F-L, Su H-B. Extracorporeal High Intensity Focused Ultrasound Ablation in the Treatment of Patients with Large Hepatocellular Carcinoma. Ann Surg Oncol. 2004 Dec;11(12):1061–9.
124. Burgess A, Ayala-Grosso CA, Ganguly M, Jordão JF, Aubert I, Hynynen K. Targeted Delivery of Neural Stem Cells to the Brain Using MRI-Guided Focused Ultrasound to Disrupt the Blood-Brain Barrier. PLoS ONE [Internet]. 2011 Nov 16 [cited 2016 Sep 13];6(11). Available from: http://www.ncbi.nlm.nih.gov/pmc/articles/PMC3218061/
125. Wei K-C, Chu P-C, Wang H-YJ, Huang C-Y, Chen P-Y, Tsai H-C, Lu Y-J, Lee P-Y, Tseng I-C, Feng L-Y, Hsu P-W, Yen T-C, Liu H-L. Focused Ultrasound-Induced Blood–Brain Barrier Opening to Enhance Temozolomide Delivery for Glioblastoma Treatment: A Preclinical Study. He X, editor. PLoS ONE. 2013 Mar 19;8(3):e58995.